

## NUMERICAL ANALYSIS OF A CROSS-FLOW FAN WITH TWO OUTLETS

Mekonnen Gebreslasie Gebrehiwot<sup>1,2,\*</sup> Josse De Baerdemaeker<sup>1</sup>, Martine Baelmans<sup>2</sup>

<sup>1</sup> Division of Mechatronics, Biostatistics and Sensors (MeBioS), Department of Biosystems, K.U.Leuven, Kasteelpark Arenberg 30, B-3001 Heverlee, Belgium

<sup>2</sup> Department of Mechanical Engineering, K.U.Leuven, Celestijnenlaan 300A, Heverlee 3001, Belgium

\* Corresponding author

Tel: +32 16 322546, Fax: +32 16 322985

Email: mekonnen.gebreslasie@biw.kuleuven.be

### ABSTRACT

Cross Flow Fans (CFFs) are used in air conditioning and ventilation technology because of their compact design and low noise. In addition, CFFs can provide a uniform velocity profile along the width of the fan. This offers an enormous advantage in applications with large width to diameter ratios as needed. However, as the flow pattern inside a CFF is very complex, classical fan design is not applicable. At present, the design of CFFs is most often based on experimental investigation and empirical experience. In order to investigate the behaviour of these type of fans and its relation to the complex flow structure inside casing and rotor, CFD-simulations are carried out. In this study, transient solutions for a two dimensional viscous and incompressible model of the fan are used to assess the cross flow fan with two parallel outlets. The impact of the outlet configuration on the flow patterns is thereby numerically investigated. It is shown that both the diffuser and the position of the vortex wall play a crucial role to achieve stable and balanced volumetric flows through the two outlets.

### NOMENCLATURE

$\rho$	[Kg/m <sup>3</sup> ]	Density
$P_s$	[Pa]	Static pressure
$P_d$	[Pa]	Dynamic pressure
$P_t$	[Pa]	Total pressure
$D_1$	[m]	Internal diameter of impeller
$D_2$	[m]	External diameter of impeller
$Q$	[m <sup>3</sup> /s]	Flow rate
$u_2$	[m/s]	Blade tip speed
$L$	[m]	Axial length of the fan
$\varphi = \frac{Q}{LD_2u_2}$	[-]	Non dimensional flow coefficient
$\psi = \frac{P}{0.5\rho u_2^2}$	[-]	Non dimensional pressure coefficient
$Y^+$	[-]	Non dimensional wall coordinate

### INTRODUCTION

Cross-flow fans (CFFs) are a particular type of fans having a drum-type impeller with a high external to internal diameter ratio. Impeller lengths can be varied almost at will in order to obtain the desired flow rate. This feature allows rotational speed not to be increased to enhance the flow rate and makes cross-flow fans particularly suitable for applications in which radial room is limited or low noise levels are prescribed. They are a unique type of turbomachinery in the sense that both suction and discharge occur radially. An ordinary CFF consists of a cylindrical rotor, forward curved blades, and a closed ended casing with suction side inflow, rear wall contour, vortex wall and pressure side outlet. The air radially flows from the suction side into the blades, passes through the rotor centre and discharges at the opposite side of the rotor. Thus, the flow field configuration is characterized by the double passage of the air through the impeller blades. Hereby a vortex is formed within the impeller. Its position and strength deeply affects the fan performance. In turn, the internal flow field is affected by both impeller and casing geometry. Figure 1 shows the flow field configuration of a general cross-flow fan [15].

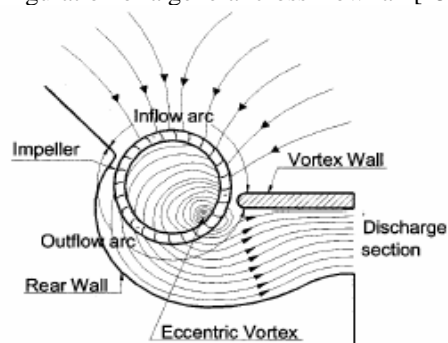
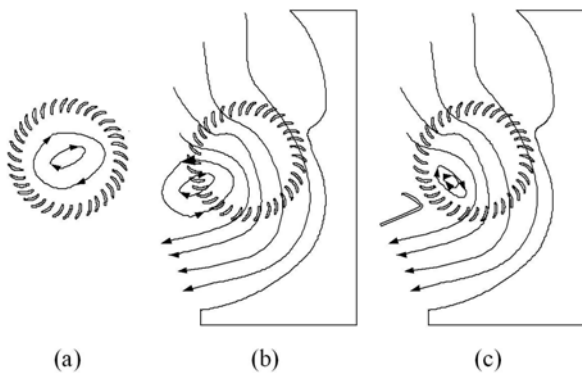


Figure 1: CFF Flow field configuration

Understanding the development of the internal flow in a CFF is helpful to improve its performance. According to

[13], the development of the eccentric vortex in a cross-flow fan is governed by three important features: (a) the rotor rotation, (b) the addition of a rear wall and (c) the introduction of a vortex wall or so-called tongue. When the rotor rotates alone, a vortex is formed inside the centre of the rotor (see figure 2), and the flow field is almost symmetrical. Addition of the rear wall pushes away the vortex from it, and the flow field becomes asymmetrical. Placing the vortex wall near the rotor moves the vortex towards it, leading to a so called “eccentric vortex”. The centre of the eccentric vortex is inside the rotor near the internal periphery of the impeller. This effects a transient flow in the blade channels. As a result, the internal flow of CFF is divided into two regions: the eccentric vortex flow consisting of completely closed stream lines at one hand and the transverse flow with in and outflow on the other.



**Figure 2:** CFF vortex development

According to previous studies [3,9,11], the design of the internal flow duct, including both components of rear wall and tongue, plays a key role on the CFF performance. Therefore, recent experimental research focused on improved designs of the internal flow duct in CFFs [7,8,12,14,16]. Thus, experimental evidence is obtained that the CFF performance primarily depends upon the position and the total pressure of the vortex centre. Further, the most serious criticism for the design of CFF is that there are no universal laws to follow. In this context, [12] measured both internal velocity and pressure distributions of several CFFs with geometrical similarity. They proposed a universal form of CFF performance based upon the relation of the reduced flow coefficient and the reduced total pressure rise coefficient. Furthermore, [7] tested the performance of five impellers with similar shape but different dimensions operating at various rotational speeds. They found that similarity laws apply for CFFs when the operating Reynolds number is above the critical Reynolds number. Recent researches, [13], used the similarity laws by [7]. In this paper, the dimensionless parameters according to these scaling laws are used to present all results.

Although most studies thus far adopted experimental methods to investigate CFF performance, also more cost effective numerical studies on predicting the internal flow fields of CFFs have been successfully performed [1,2,5,10]. The use of Computational Fluid Dynamics (CFD) for the computation of turbomachinery flows has significantly increased in the past years. Amongst other, [6,10,13] have demonstrated the accuracy of CFD for CFF performance prediction. Furthermore, combined with measurements, CFD provides a complementary tool for simulation, design, optimization and analysis of the flow field inside a turbomachine.

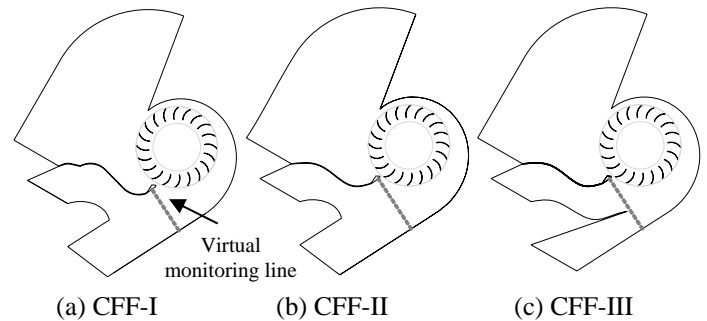


**Figure 3:** Geometrical configuration of all CFFs

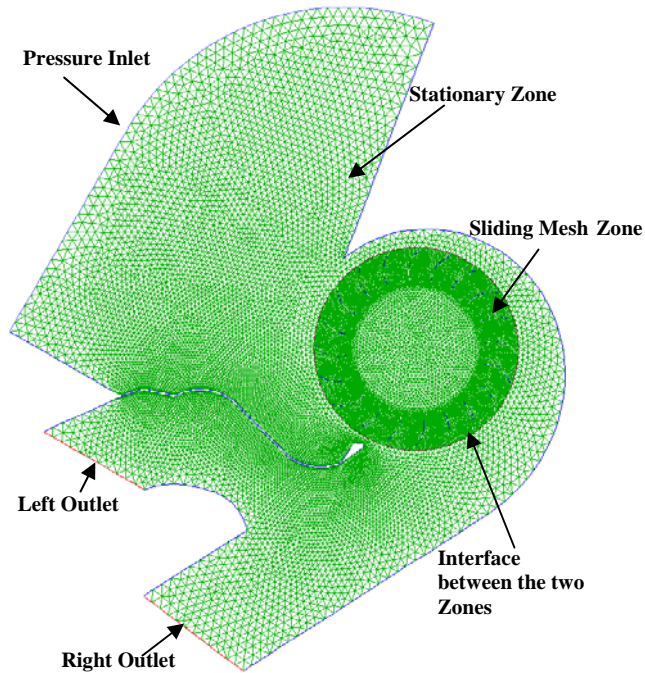
In this paper, CFD is utilized to investigate the influence of different outlet configurations on the performance of a CFF impeller. All outlet configurations consist of two parallel outlets. The objective is to achieve a balanced flow division between the two outlets through the modification of the outlet duct configuration and the position of the vortex wall.

## NUMERICAL SETUP FOR THE CFFs

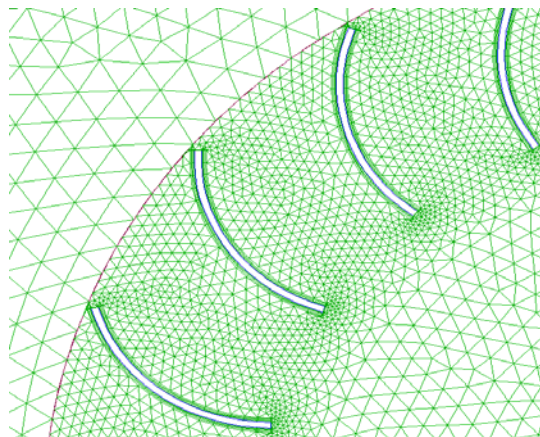
### Geometrical Model Setup and Mesh Generation

In this research, three CFFs, namely CFF-I, CFF-II and CFF-III, of the same dimension but with changes in vortex wall position and outlet duct configuration are considered. All CFFs geometries have the same impeller of 20 forward curved blades at a uniform pitch and with an external to internal diameter ratio  $D_2/D_1$  of 1.42. As the CFFs under investigation are meant for use with a relatively large axis measure, a 2-dimensional numerical approach can be justified. The difference in casing geometry of all CFFs can be seen in Figure 3. In CFF-II the upper wall in the left outlet is slightly smoothed and the position of the vortex wall is moved  $18^\circ$  clock wise with respect to CFF-I. In CFF-III, the splitter between the outlet ducts is made sharp and extruded towards the rotor in addition to the changes made in CFF-II. The geometrical models and their meshes are generated using GAMBIT<sup>®</sup>. Finer elements are used in the rotating zone and in the boundary layer near all walls ensuring  $30 < Y^+ < 300$ . Figure 4 shows computational domain of CFF-I and the boundary conditions. The grid consists of a total

of 39148 triangular cells are generated, of which 24168 cells are used in the rotating zone and 14980 cells in the stationary zone.



(a) Global Grid



(b) Local Grid near the blades

Figure 4: Grid system and definition of boundary conditions

### Modelling Aspects and Numerical Approach

As the CFF under investigation is meant for use with large axis measures, a 2-dimensional approach can be justified. Further, the calculation is performed unsteady, because of the highly transient flow in the blade channels. Thus, in order to assess the CFF performance with parallel outlets, the transient, 2-dimensional, viscous, incompressible Navier-Stokes equations are solved. Moreover, the RNG  $k - \varepsilon$  is used as a turbulence model. The pressure correction is realized with the

SIMPLE algorithm. Regarding the boundary conditions, no-slip condition and standard wall functions are used at walls and impeller blades. At the inlet and outlet, constant static pressure is presumed. The rotational speed of the moving zone is assumed to be 900 rpm.

The CFD software FLUENT is utilized to simulate the internal airflow distribution of the three CFFs. For unsteady calculations, the solution using the multiple reference frames technique is used as an initial condition. The sliding mesh technique is then used to obtain the final unsteady results. Thus, the whole fan including its rotor-stator interaction is modelled.

### Grid Sensitivity

Grid independence has been examined using four different grids on CFF-I. Hereby, the grid is gradually refined from a coarse grid consisting of 24,743 elements up to the finest grid consisting of 95,201 elements. Figure 5 shows the flow coefficient  $\phi$  with grid refinement. The flow coefficient  $\phi$  between the two finest grids does not vary much, leading to an acceptable level of grid independence.

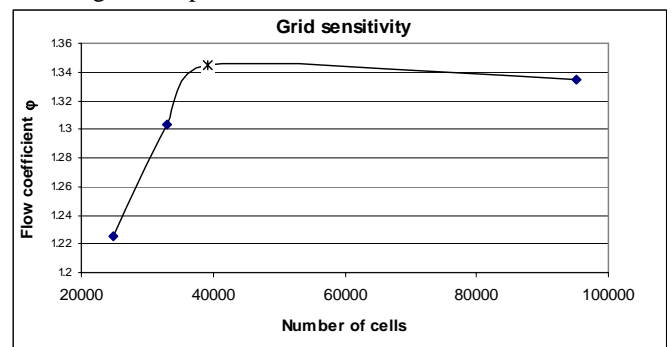


Figure 5: Grid sensitivity analysis on CFF-I

## RESULTS AND DISCUSSION

All three CFFs, are simulated with constant static pressure loads ranging from  $\psi = 0$  up to  $\psi = 1.5$  imposed at both outlets. In the next subsections the general flow features of the CFFs, their impeller and overall performance will be discussed.

### General Flow Features and Overall Performance

Figure 6 shows pressure contours of all fans at a representative load of  $\psi = 1$ . From the total pressure contours it can be seen that the impeller blades exert work on the fluid during both passages through the blades. For the dynamic pressure plots, it can be seen that at the rear wall edge of CFF-I the flow is partially blocked. This blockage has clearly been removed by widening the outlet opening of the fan in CFF-II and CFF-III. Simultaneously, a lower pressure region is created just below the rear wall edge (see also Figure 1) in these configurations.

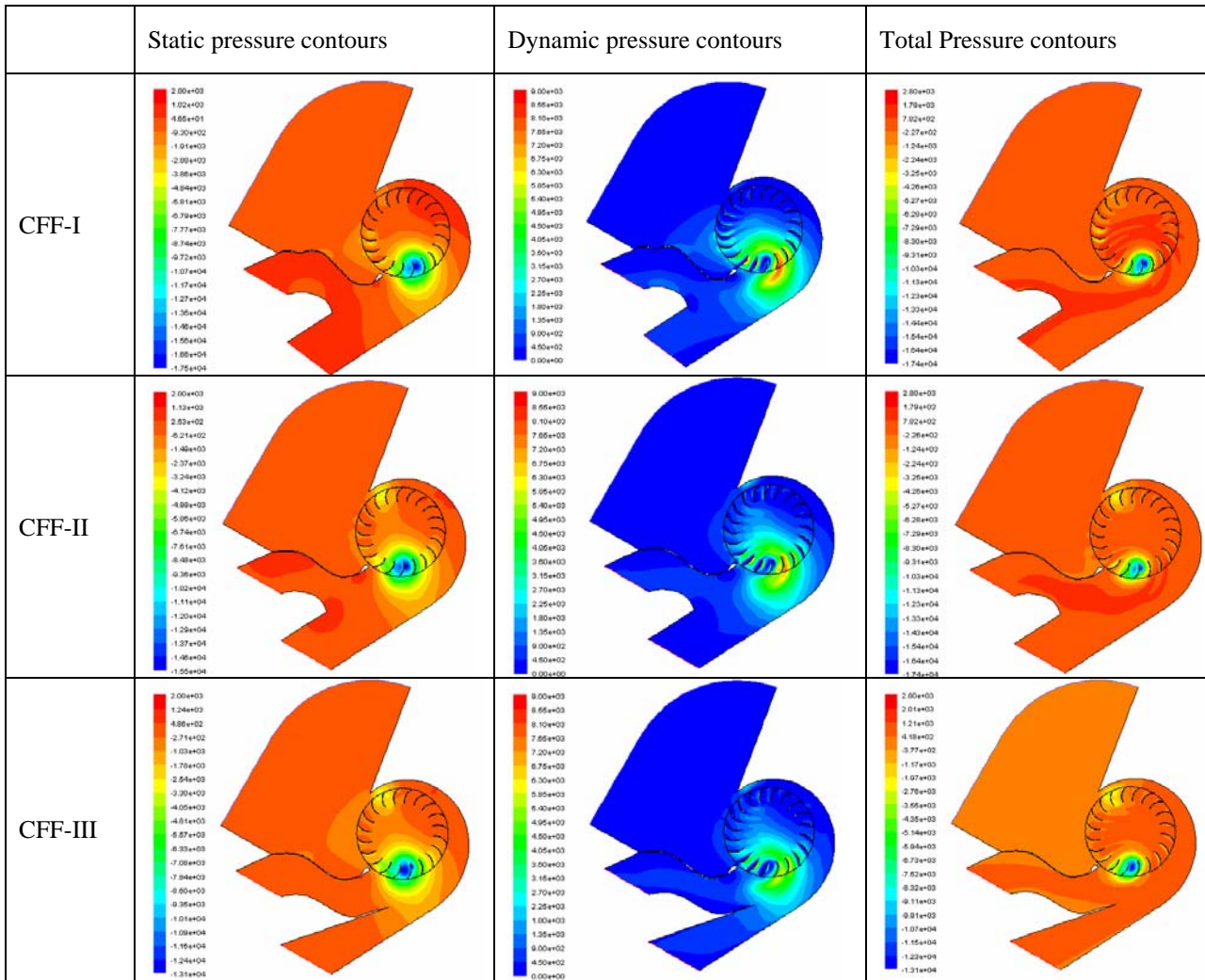


Figure 6: Representative pressure contour plots of all CFFs

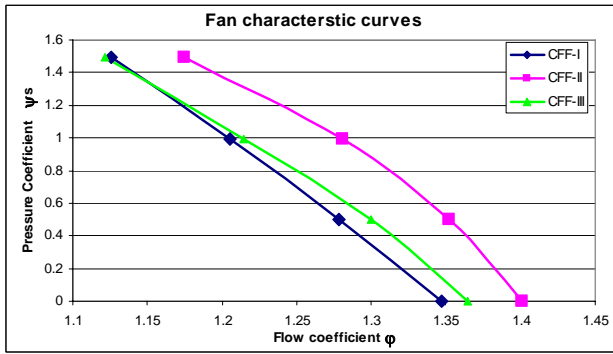
The general fan characteristic curves of the three CFFs and the air flow division between the two outlets is shown in Figure 7. From Figure 7(a), it can be seen that all configurations exhibit stable rotor performance with respect to the load. The overall performance of CFF-II is better than CFF-I: the flow rate for CFF-II is slightly higher than the other fans at the same load. It should however be noted that this effect amounts only to 3%. Further, this feature can only be partially explained by the wider outlet opening. Indeed, an alteration in outlet duct, as performed in CFF-III already cancels out this advantage.

From figure 6, it can be also observed that the centre of the eccentric vortex moves with the vortex wall position. However, the position of the eccentric vortex relative to the vortex wall is not much affected by the changes in the outlet duct and vortex wall position. More exact post processing in the contour plots show that the centre of the vortex is positioned at about 50° counter clockwise from

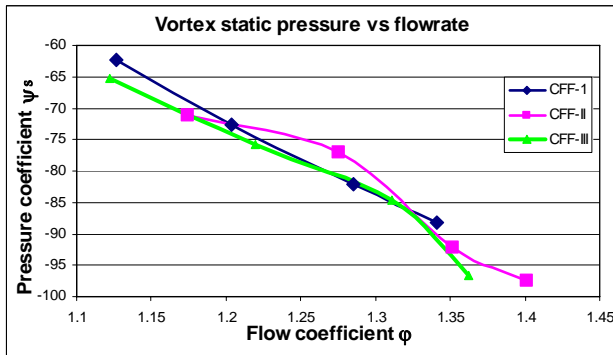
the vortex wall. As such a wider outlet opening induces also a larger available cross-sectional area for the transverse flow. The lowest pressure (negative pressure) within the whole centrifugal fan exists in the centre of this vortex. The behaviour of the static pressure coefficient of  $\psi_s$  at the centre of the vortex with respect to the flow coefficient  $\phi$  from the CFFs is shown in Figure 7(b). Comparison between the curves shows that the change in position of the vortex wall (CFF-II), which increased the impeller outlet area, has brought a decrease in the vortex centre static pressure. Furthermore, the static pressure in the vortex eye seems to be very sensitive to the total mass flow or flow coefficient. This confirms the findings by [13].

In global it can be concluded that the different outlet configurations only marginally affect the CFF performance. However, as will be explained in the next sections, these geometrical aspects largely influence the

load balance between the two parallel outlet flows. To investigate this influence the impeller performance for different outlet configurations will be first assessed.



(a)



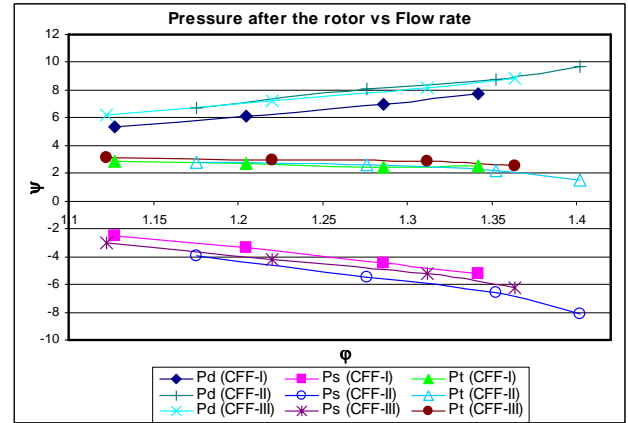
(b)

Figure 7: (a) Fan characteristic curves and (b) Vortex static pressure versus flow coefficient

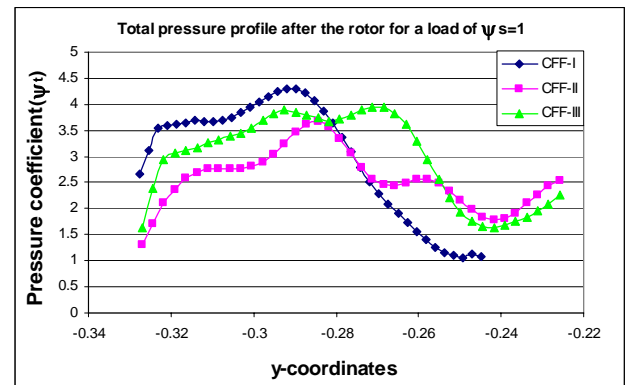
### Impeller performance for different outlet configurations

To assess the impeller performance under the three casing conditions under consideration, the dynamic, static and total pressures are computed right after the impeller in a virtual monitoring line shown in Figure 3(a) for all the fans. The resulting area averaged pressure coefficient along the line is plotted with respect to the flow coefficient in Figure 8(a). The increase in total pressure over the rotor is only marginally changing with mass flow relative to the changes observed in dynamic pressure and static pressure. In addition, neither the changes in outlet duct geometry nor the position of the vortex wall have influenced the total pressure build up by the impeller. Figure 8(b) shows the total pressure profiles on the virtual monitoring line after the impeller (from bottom to top) for the representative load of  $\psi_s = 1$ . It shows that the increase in rotor outlet area achieved due to movement of the vortex wall, in CFF-II and CFF-III has made the total pressure distribution along the line more homogeneous as compared to CFF-I. This feature is clearly linked to both the more uniform flow conditions in the outlet ducts as well as a more homogeneous flow

at the rotor inlet. The latter is connected with the introduction of a more pronounced vortex at the rear wall and less flow blockage at the rotor inlet.



(a)



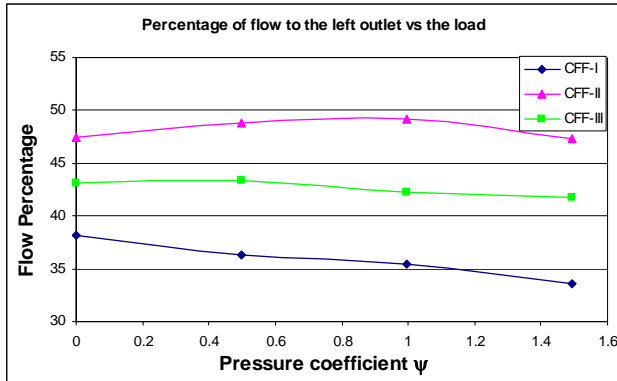
(b)

Figure 8: (a) Pressures after the rotor with respect to mass flow rate (b) Total pressure profile after the rotor for a load of  $\psi_s = 1$

### Flow balancing over the parallel outlets

The relative air flow contribution through the left outlet is shown in Figure 9. It shows that in CFF-I more air flows through the right outlet and the left outlet gets only about 35% of the flow. The share of the left outlet duct is improved to 47% and 43% in CFF-II and CFF-III respectively. As CFF-I and CFF-II only differ in the position of the vortex wall; one can conclude that the mass flow rate division between the two outlets can be largely influenced by the rotor outlet opening. This can be explained by the fact that a larger outlet opening prevents flow blockage at the inlet and creates a more uniform total pressure profile at the rotor outlet as discussed above. Furthermore, changing outlet duct area ratios can further affect the flow balance between the two flows, as can be seen from differences between CFF-II and CFF-III. This can be explained by the fact that the total pressure at the outlet (see Figure 6(a)) is only marginally affected by the outlet configuration. Thus, the

flow balance can be easily achieved by altering the outlet ducts areas near the rotor outlet.



**Figure 9:** Flow contribution through the upper outlet

## CONCLUSIONS

Computational Fluid Dynamics has been used to predict the internal flow fields of three CFFs with the same rotor but different shapes of the outlet ducts and positions of the vortex wall. The rotor performance for these configurations was assessed. Special attention was paid on the effect of the geometric changes with respect to the position and static pressure of the eccentric vortex centre and on achieving a balanced air flow division between the two outlets. According to the numerical results, the following conclusions can be made.

The rotor exhibits a stable performance with respect to the load under all configurations. It has been observed that the increase in total pressure over the rotor was only marginally changing with mass flow relative to the changes observed in dynamic pressure and static pressure. In addition, neither the changes in outlet duct geometry nor the position of the vortex wall has influenced the total pressure build up by the impeller. However, the increase in rotor outlet area created by the change in position of the vortex wall has resulted in a more uniform total pressure along the rotor outlet. It has been observed that the eccentric vortex moves with the vortex wall. The position of the eccentric vortex relative to the vortex wall is not affected by the changes made in the geometry; the vortex stays at about 50° counter clockwise from the tip of the vortex wall in all cases. However, the static pressure of the eccentric vortex is decreased by the changes in position of the vortex wall. This is related to an increase in mass flow rate. A more uniform air division between the two outlets is obtained by the changes made in the ducts and the vortex wall. It is observed that the mass flow rate division between the two outlets can be largely influenced by the rotor outlet opening. This can be explained by the fact that a larger outlet opening prevents flow blockage at the inlet. Furthermore, changing outlet duct area ratios can further affect the flow balance between the two flows.

## REFERENCES

- [1] Bert P.F., Pessiani M., Combes J.F. and Kueny J.L. 1996. Unsteady flow calculation in a cross-flow fan using a finite element method. ASME Paper 96-GT-443.
- [2] Dornstetter S., 2002. Numerische und experimentelle Untersuchungen an Querstrom ventilatoren. Dissertation, TU Karlsruhe.
- [3] Eck, B. Fans, 1973 (Pergamon Press, Oxford).
- [4] FLUENT Inc, 1997. Validating the New Sliding mesh Model in FLUENT/UNS, *FLUENT Newsletter* Vol.6 (2) pp. 12
- [5] Fukano T., Chen C., and Hara Y. 1995. A numerical analysis of flow in a cross-flow fan. *Numerical Simulations in Turbomachinery. Proceedings of the ASME, FED-Vol.227*, 53-58.
- [6] Gabi M. and Klemm T. 2004. Numerical and Experimental Investigations of Cross-Flow Fans. *Journal of Computational and Applied Mechanics*, Vol. 5, No. 2, pp. 251-261
- [7] Lazzaretto L., Lazzaretto A., Martegani A.D. and Macor A. 2001. On cross flow fan similarity effect of casing shape. *ASME Journal of Fluids Engineering*, Vol. 123, 523-531
- [8] Matsuki K., Shinobu Y. and Takushima A., 1988. Experimental Study of Internal Flow of a Room Air Conditioner Incorporating a Cross-flow Fan, *ASHRAE Transactions*, Vol. 94, 450-364.
- [9] Mazur J. and Singh T., 1987. Effects of Speed, Blade End Conditions, and Measurement Probes on Performance of a Cross Flow Fan. *ASME Winter Annual Meeting*, No. 87-WA/FE-2
- [10] Moon Y.J., Cho Y., and Nam H.S., 2003. Computation of unsteady viscous flow and aero acoustic noise of cross-flow fans. *Computers & Fluids*, Vol. 32, pp. 995-1015.
- [11] Murata S.I., and Nishihara K., 1976. An Experimental Study of Cross Flow-1st Report, Effects of Housing Geometry on the Fan Performance, *Bull. JSME*, Vol. 19, No. 129, pp. 461-471.
- [12] Tanaka S. and Murta S., 1995. Scale effect in cross flow fans: Effect of fan dimensions on flow details and the universal representation of performances. *JSME International Journal, Series B* 38(3):388-397.
- [13] Shih Y.C., Hou H.C., and Chiang H., 2004. Numerical Study of the Similarity Law for the Cross Flow Fan of the Split-Type Air Conditioner, *ASHRAE Transactions*, Vol. 110, Part II, pp.378-388..
- [14] Takushima A., Shinobu Y., Tanaka S. and Matsuki K., 1990. Flow measurement by laser Doppler velocimeter in a cross-flow fan for air-conditioning use. *ASHRAE Transactions* 96(1):497-501.
- [15] Toffolo A., Lazzaretto A. and Martegani A. D., 2004. Cross-flow fan design guidelines for multi-objective performance optimization. *Proc. Instn Mech. Engrs: J. Power and Energy*, Vol. 218A, 33-42.
- [16] Tsuruski H., Tsujimoto Y., Yoshida Y. and Kitagawa K., 1997. Visualization measurement and numerical analysis of internal flow in cross-flow fan. *ASME, Journal of Fluids Engineering*, Vol. 119, pp. 633-638.